

Unusual Exchange Couplings and Intermediate Temperature Weyl State in $\text{Co}_3\text{Sn}_2\text{S}_2$

Qiang Zhang^{1,*}, Satoshi Okamoto^{2,3,†}, German D. Samolyuk², Matthew B. Stone¹, Alexander I. Kolesnikov¹, Rui Xue⁴, Jiaqiang Yan², Michael A. McGuire^{2,3}, David Mandrus^{5,2,4}, and D. Alan Tennant^{2,6,3}

¹Neutron Scattering Division, Oak Ridge National Laboratory, Oak Ridge, Tennessee 37831, USA

²Materials Science and Technology Division, Oak Ridge National Laboratory, Oak Ridge, Tennessee 37831, USA

³Quantum Science Center, Oak Ridge, Tennessee 37831, USA

⁴Department of Physics & Astronomy, The University of Tennessee, Knoxville, Tennessee 37996, USA

⁵Department of Materials Science and Engineering, The University of Tennessee, Knoxville, Tennessee 37996, USA

⁶Shull Wollan Center, Oak Ridge National Laboratory, Oak Ridge, Tennessee 37831, USA

 (Received 11 February 2021; revised 17 June 2021; accepted 16 July 2021; published 7 September 2021)

Understanding magnetism and its possible correlations to topological properties has emerged to the forefront as a difficult topic in studying magnetic Weyl semimetals. $\text{Co}_3\text{Sn}_2\text{S}_2$ is a newly discovered magnetic Weyl semimetal with a kagome lattice of cobalt ions and has triggered intense interest for rich fantastic phenomena. Here, we report the magnetic exchange couplings of $\text{Co}_3\text{Sn}_2\text{S}_2$ using inelastic neutron scattering and two density functional theory (DFT) based methods: constrained magnetism and multiple-scattering Green's function methods. $\text{Co}_3\text{Sn}_2\text{S}_2$ exhibits highly anisotropic magnon dispersions and linewidths below T_C , and paramagnetic excitations above T_C . The spin-wave spectra in the ferromagnetic ground state is well described by the dominant third-neighbor “across-hexagon” J_d model. Our density functional theory calculations reveal that both the symmetry-allowed 120° antiferromagnetic orders support Weyl points in the intermediate temperature region, with distinct numbers and the locations of Weyl points. Our study highlights the important role $\text{Co}_3\text{Sn}_2\text{S}_2$ can play in advancing our understanding of kagome physics and exploring the interplay between magnetism and band topology.

DOI: [10.1103/PhysRevLett.127.117201](https://doi.org/10.1103/PhysRevLett.127.117201)

The kagome lattice has attracted considerable interest since it can host new exotic magnetic and electronic states such as spin liquids [1,2] and topological Dirac or Weyl fermions [2–4]. Determination of the exchange couplings that control the magnetic phases is key to understanding these exotic states. While initial understanding of kagome magnetism is based on the isotropic nearest-neighbor (NN) exchange coupling [5,6], recent research reveals a necessary requirement of considering the further-neighbor interactions [7–9]. The kagome lattice with interactions beyond NN couplings tends to result in very rich magnetic phase diagrams based on theoretical predictions [9–12]. However, the experimental realizations of such materials are rare. Two interesting examples are haydeeite $\text{MgCu}_3(\text{OH})_6\text{Cl}_2$ [8,10,13] and kapellasite $\text{ZnCu}_3(\text{OH})_6\text{Cl}_2$ [8,13–15], where the third-neighbor interaction competes with the NN one. Dominant third-neighbor exchange “ J_3 ” was discovered in antiferromagnetic (AFM) $\text{BaCu}_3\text{V}_2\text{O}_8(\text{OD})_2$ [16] along with a very weak third-neighbor “across-hexagon” J_d . Identifying new magnetic kagome materials with significant further-neighbor interaction is therefore of great interest to advance the field of kagome physics and to explore the emergent phenomena in such materials.

The discovery of new magnetic Weyl semimetal $\text{Co}_3\text{Sn}_2\text{S}_2$ with a kagome lattice of cobalt ions has triggered

tremendous interest to explore fantastic phenomena and underlying physics [4,17–20]. $\text{Co}_3\text{Sn}_2\text{S}_2$ exhibits tunable magnetic states associated with anomalous Hall conductivity, and an exotic Weyl state at low temperatures [4,21]. The ground state of ferromagnetic (FM) order with moments along the c axis exists below $T_A \approx 130$ K, as shown in Fig. 1(a). The FM order is believed [4,21] to be important in the breaking of time reversal symmetry (\mathcal{T}) that induces a Weyl state in $T < T_A$ in $\text{Co}_3\text{Sn}_2\text{S}_2$. It is therefore crucial to determine the exchange couplings of the FM ground state. There have been theoretical attempts to determine these exchange couplings. It was proposed [22] that out-of-plane NN J_z is mainly responsible for the formation of the FM order below T_A . In sharp contrast, Liu *et al.* [23] employed a multiple-scattering Green's function method to calculate the exchange couplings and obtained a dominant NN in-plane J_1 to explain the FM order. These discrepancies show the difficulty in determining the precise exchange couplings and point to the need for careful experimental measurements to help constrain theoretical models and further our understanding and development of this material. Furthermore, recent investigations [24–26] revealed the existence of an anomalous phase showing peculiar properties like magnetic relaxation in the intermediate temperature region $T_A < T < T_C$. A coexistence of the ferromagnetic (FM) order and an AFM order was

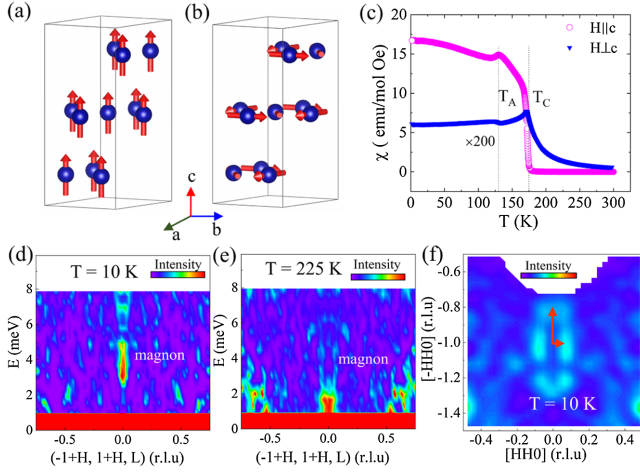


FIG. 1. Magnetic structures of $\text{Co}_3\text{Sn}_2\text{S}_2$: (a) FM order in $T < T_A$. (b) The proposed 120° AFM order in $T_A < T < T_C$ in Ref. [21]. (c) The temperature dependence of the susceptibility with field parallel to ab plane and c axis in a field of 250 Oe. Low energy magnetic excitations with $E_i = 15$ meV near FM zone center $(-1, 1, 1)$ at (d) 10 K and (e) 225 K. (f) Constant- E slice in the $(H, H, 0)$ - $(-H, H, 0)$ plane around E of 16 meV.

then uncovered by the μSR technique [21], with an in-plane 120° order proposed [see Fig. 1(b)]. It would be very important to explore if there exists a correlation between different magnetic orders and band topology and whether $\text{Co}_3\text{Sn}_2\text{S}_2$ could host a new Weyl state in $T_A < T < T_C$.

In this Letter, by a combined use of inelastic neutron scattering and linear spin-wave (SW) theory, we find that the FM ground state of $\text{Co}_3\text{Sn}_2\text{S}_2$ is stabilized by the third-neighbor “cross-hexagon” J_d , which makes $\text{Co}_3\text{Sn}_2\text{S}_2$ the first example of a kagome material exhibiting such an unusual magnetic interaction. This is compared with the exchange couplings extracted from our two density functional theory (DFT) based methods: one is a constrained magnetism method to compare the total energy of magnetically ordered states and the other utilizes multiple-scattering Green’s function methods considering small spin reorientations from the magnetic ground state. Using DFT, we compare the electronic band structures associated with FM order and the two possible symmetry-allowed 120° AFM orders. Distinct Weyl points are found to exist for $T_A < T < T_C$ associated with the two different 120° AFM orders, indicating that a new Weyl state may exist in this temperature region.

The details of sample preparation and characterization, neutron scattering experiments, spin-wave analysis using the SpinW package, and DFT calculations can be found in the Supplemental Material (SM) [27]. Our neutron diffraction experiment at 10 K confirms the reported rhombohedral structure with space group of $R\bar{3}m$ (No. 166) [4,24,26,39]. The temperature dependence of susceptibility of the single crystal in Fig. 1(c) exhibits two anomalies at $T_C \approx 175$ K and $T_A \approx 130$ K. The field dependence of

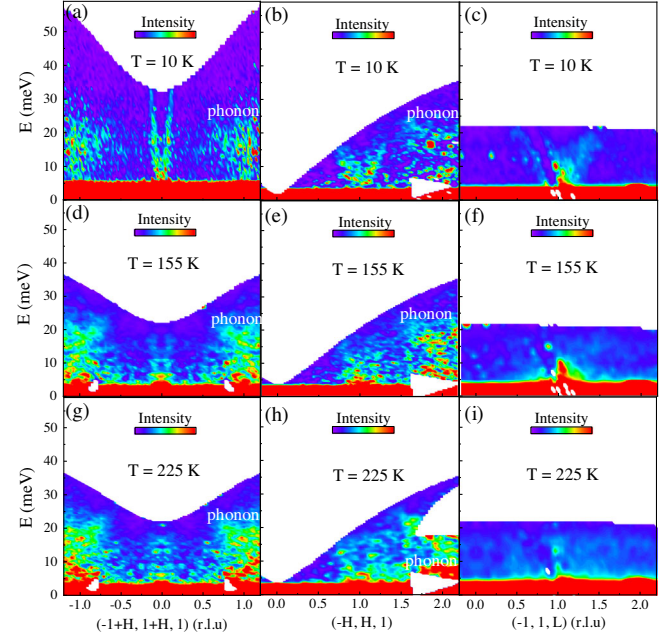


FIG. 2. Magnetic excitations near magnetic zone center $(-1\ 1\ 1)$ along $[\text{HH}0]$, $[-\text{HH}0]$, and $[00L]$ direction at (a)–(c) 10 K, (d)–(f) 155 K, and (g)–(i) 225 K. Phonons were also observed at higher Q zones.

magnetization in Fig. S2(b) [27] shows an easy direction along the c axis with a moment $\approx 0.37\mu_B$, consistent with the FM order reported previously [21,24]. In Figs. 1(d) and 1(e), we compare the low- E magnetic excitations near the FM zone center $(-1, 1, 1)$ at 10 and 225 K, respectively. A clear spin gap $E_g \approx 2.3$ meV is observed at 10 K, consistent with the previous report [23]. The data at 225 K are consistent with a gapless spectrum when the long-range magnetic order disappears.

The magnetic excitations along in-plane $[\text{HH}0]$, $[-\text{HH}0]$ and out-of-plane L directions at 5, 155, and 225 K near $(-1, 1, 1)$ are displayed in Figs. 2(a)–2(i). Phonons with energy ≈ 18 meV at zone boundaries are also observed in these figures and Fig. S3(a) [27]. At 10 K in the FM state, a remarkable feature is that the dispersion along the $[\text{HH}0]$ direction is much steeper yielding a much larger dE/dQ slopes than the $[-\text{HH}0]$ (or equivalent $[\text{H}00]$) direction, as can also be seen from the very anisotropic excitations in constant- E slice in Fig. 1(f). The dispersion along the L direction shows much smaller slopes than the $[\text{HH}0]$ directions too, with $E < 30$ meV at the zone boundary $(-1, 1, 1.5)$. Furthermore, the SWs along $[\text{HH}0]$ are very sharp and become broader along $[-\text{HH}0]$. In addition, significant SW broadening is observed along the L direction. Our results show that $\text{Co}_3\text{Sn}_2\text{S}_2$ exhibits significant anisotropy in both magnon dispersions and linewidths. Additionally, a strong SW damping is observed as Q approaches the zone boundaries along these three directions (see Fig. S3(b–d) in the SM [27]). In Ref. [23], only the low- E SW dispersions along $[\text{H}00]$ and $[00L]$ near the

(003) zone were reported below ≈ 18 and 15 meV, respectively. Our SW dispersion along the same [00L] direction is similar to that report. At 155 K, the FM SWs are still visible and become broader without obvious change in the slopes of the dispersions. At 225 K within the paramagnetic state, the dispersions disappear, and evolve into diffuse inelastic signal indicative of the existence of paramagnetic excitations.

To quantitatively determine the magnetic interactions of the FM ground state in $\text{Co}_3\text{Sn}_2\text{S}_2$, we have fitted the experimental dispersions and intensities of the SW at 10 K using the *SpinW* package [28] for the following spin Hamiltonian:

$$H = \sum_{i,j} J_{ij} \mathbf{S}_i \cdot \mathbf{S}_j + \sum_{\alpha,\beta,i} S_i^\alpha A_i^{\alpha\beta} S_i^\beta, \quad (1)$$

where \mathbf{S}_i is a spin operator, J_{ij} is an exchange coupling between spins, and $A_i^{\alpha\beta}$ is a 3×3 matrix representing the single-ion anisotropy. The J_{ij} bonds are illustrated in Fig. 3(e). We have considered in-plane exchange couplings NN J_1 , next NN (NNN) J_2 , third-neighbor J_3 , inequivalent third-neighbor ‘‘across-hexagon’’ J_d in the kagome lattice, as well as out-of-plane exchange couplings J_{c1} , J_{c2} , and J_{c3} for both FM and AFM signs in the fits. Extensive effort has been made to consider all the possible models (see the details in the SM [27]). Only the model with dominant FM ‘‘across-hexagon’’ J_d leads to good fits to experimental SW dispersions as shown in Fig. 3(a). Although we do not consider the SW damping, the intensities of the simulated SW spectra $S(Q, E)$ shown in Fig. 3(b) are consistent with the experimental results. The optimized magnetic exchange couplings are summarized in Table I, which includes the strongest FM J_d , FM J_{c1} , FM J_{c2} , and very weak AFM J_2 . Attempts to use other models fail to reproduce the very different slopes dE/dQ of the in-plane SW dispersions. Note that the strengths of the third-neighbor SJ_3 and SJ_d are very different and the J_1 and J_3 are negligible. The AFM NNN J_2 exchange is weak but serves to provide frustration with a long-range dominant FM coupling over the diagonal of the kagome hexagons. The single-ion anisotropy term SA_i contributes to the emergence of the spin gap.

Experimental spin wave dispersions are used to critique the exchange couplings extracted from the currently popular theoretical approaches. We carried out DFT calculations and confirmed the FM ordering with symmetry $R\bar{3}m'$ is most stable as observed experimentally. The ordered Co moment is found to be $\approx 0.35\mu_B$ ($S \approx 0.17$), well consistent with the experimental results. We then examine exchange couplings theoretically. First, we employ the constrained magnetism method and find SJ_2 is the strongest one. Second, we use a magnetic force theorem within multiple scattering theory (MFMST) [40,41] and the resultant exchange couplings belong to dominant J_1 model. The

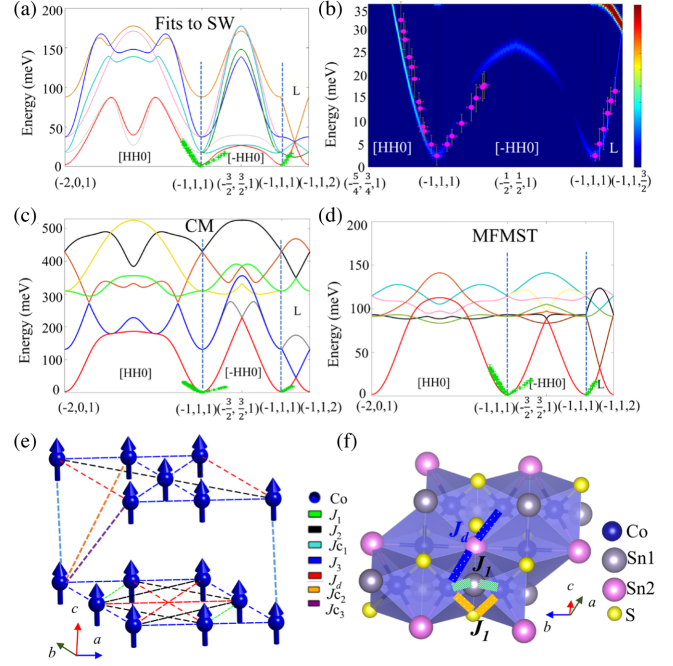


FIG. 3. Simulation on (a) SW dispersions and (b) intensity after the convolution to the instrument resolution ≈ 2 meV using the exchange couplings from the fits to experimental SWs. The dot symbols show the experimental SW dispersions. Simulated SW dispersions using the exchange coupling from (c) the constrained magnetism (CM) method and (d) MFMST to illustrate the inability of such calculations to capture the high anisotropy in the experimental SW dispersions. For a better comparison, the same anisotropic term SA of 1.36 was used in all the simulations to reproduce the experimental spin gap. (e) Illustration of Co—Co exchange couplings and the spin configurations. (f) Illustration of compressed octahedral environment of cobalt, geometrical representation of possible exchange pathways Co—S—Co, Co—Sn1—Co for J_1 and Co—Sn(2)—Co for J_d .

magnetic exchange couplings were also reported in Ref. [23] by employing a combination of the magnetic force theorem [40] and Wannier functions approach (MFWF) [42], which belongs to the dominant J_1 model too. The magnetic exchange couplings obtained from these three theoretical methods are summarized in Table I.

The simulated SW dispersions using these exchange couplings are displayed in Figs. 3(c) and 3(d) and Fig. S4 in the Supplemental Material [27], respectively. The theoretical SW dispersions significantly deviate from the experimental results, indicating these three methods have shortcomings for extracting the reliable exchange couplings in $\text{Co}_3\text{Sn}_2\text{S}_2$. The main reason is that $\text{Co}_3\text{Sn}_2\text{S}_2$ is a weakly correlated itinerant system with small moment in which the size of magnetic moment depends on its deviation from ground state. However, DFT calculations use rigid spin approximation, i.e., moment size independent from its orientation. Constrained magnetism calculations overestimate the exchange coupling because these calculations necessarily force ordered moments for metastable

TABLE I. Summary of the exchange couplings with unit of meV obtained using different approaches. A negative (positive) sign indicates ferromagnetic (antiferromagnetic) coupling.

Approach	SJ_1	SJ_2	SJ_3	SJ_d	SJ_{c1}	SJ_{c2}	SJ_{c3}	Reference
Fits to SW spectra		5.78		-29.94	-11.56	-1.70		This Letter
Constrained magnetism	-13.8	-36.3	-4.95	-4.95	-31.65	-13.65	15.3	This Letter
MF MST	-7.4118	0.1176	-1.2941	-3.6471	-0.3529	-5.0588	-3.5294	This Letter
MF WF	-13.94	-0.9412	-0.1176	-0.1176	-1.7647	-4.4118	-0.6471	[23]

magnetically ordered states, and therefore overestimate the energy of such states. The MF MST or MF WF methods calculate the energy change due to small magnetic moment deviation from the ground state direction under the assumption that the moment size does not change and may underestimate the magnetic exchange couplings as in fcc Ni [43,44].

The dominant third-neighbor SJ_d across the hexagons is very unusual in kagome lattice systems. To shed light on it, we examine the crystal structure and discuss the possible exchange pathways. As illustrated in Fig. 3(f), the kagome lattice is formed by the cobalt atoms in the ab layer and centered by Sn(2) atoms. The cobalt atoms are octahedrally coordinated by two axial sulfur atoms and four tin atoms, i.e., two in-equivalent Sn(1) and Sn(2), with shared faces among them within the ab plane. Interestingly, the cobalt-centered octahedra are strongly compressed, with much shorter Co-S distance 2.1729 Å than Co-Sn(1) distance 2.6779 Å and Co-Sn(2) one 2.6796 Å at 10 K. There are two possible exchange pathways lying above and below the kagome (ab) layers: Co-S-Co with the bond angle of 76.14° and Co-Sn1-Co with a bond angle of 60.04°. The large difference in the bond lengths and angles may result in two competing AFM and FM magnetic interactions that cancel out, leading to a negligible J_1 like in BaCu₃V₂O₈(OD)₂ [16]. Because of the shortest distance between Co and S, they form hybridized bands, which are dominated by Co near the Fermi level, i.e., antibonding bands (see SM [27] for more details). While the Co-Sn distance is longer than the Co-S distance, Sn states are also found to contribute to the electronic bands near the Fermi level, along the Γ -T line and near the L point. The former is expected to contribute to the in-plane strongest FM J_d coupling via Co-Sn(2)-Co across the Co hexagon since $k_x = k_y = 0$, and the latter is expected to contribute to the out-of-plane exchange couplings J_{c1} and J_{c2} because of nonzero momentum.

We next examine the electronic band structure in the ground state and metastable magnetic states using the constrained magnetism method of DFT. Although this method overestimated the magnetic exchange couplings, it is expected to provide reliable electronic band structures because these are single-particle properties governed by the underlying symmetry and the current system is weakly correlated. Our electronic band structure for the FM

ordering (see Fig. S7 [27]) is indeed well consistent with the previous theoretical results [4] and experimental ARPES measurements [4]. The previous work proposed $R\text{-}3m$ 120° AFM ordering [21] in $T_A < T < T_C$. In fact, there are two symmetry inequivalent AFM structures of $R\text{-}3m$ and $R\text{-}3m'$ (same symmetry as FM order) as schematically shown in Figs. 4(a) and 4(b), respectively. We found $R\text{-}3m$ has lower energy than $R\text{-}3m'$ by ~ 1 meV per formula unit. Since the difference in energy is rather small, this suggest $R\text{-}3m'$ structure may be also considered in analyzing the electronic properties in this temperature region.

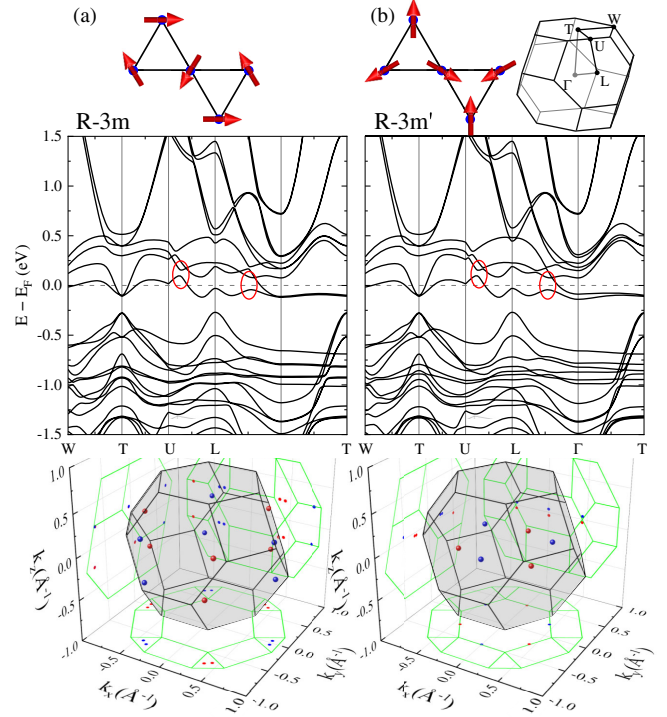


FIG. 4. Spin configuration (top panel), band structure (middle panel) and Weyl points in the first Brillouin zone (bottom panel) for (a) the $R\text{-}3m$ AFM ordering and (b) the $R\text{-}3m'$ AFM ordering. Right top figure shows the first Brillouin zone with high symmetry points. Red circles indicate the reminiscent of nodal lines in the FM state without SOC. For the $R\text{-}3m$ AFM, only Weyl points near zone boundaries are plotted. Blue (red) points in the bottom panel indicate chirality +1(-1).

The electronic band structures for the two AFM states are shown in Fig. 4. In contrast to the band structure of the FM ground state, there appear two electron pockets centered at the T point, where the two bands nearly touch. Despite their distinct band structures than that of FM order, the two AFM states have a similar feature, where two lowest conduction bands get closer along the U - L line and the L - Γ line (see red circles in Fig. 4), reminiscent of the nodal ring appearing in the FM state without the SOC. In fact, the $R\text{-}3m'$ AFM state has the combined time-reversal T and mirror-reflection \mathcal{M}_y symmetry. This symmetry protects six Weyl points in the plane running on U - L - Γ points shown in the right bottom figure in Fig. 4, as in the FM state (see detailed analysis in the SM [27]). We also found that the $R\text{-}3m$ AFM state has Weyl points. However, the locations of Weyl points are different because the combined T - \mathcal{M}_y symmetry is broken in $R\text{-}3m$ AFM. Most of these Weyl points appear near the Γ - T line, where the band structure shows nearly degenerate bands ~ 0.1 eV below the Fermi level. Another 12 Weyl points are located near zone boundaries (see the left bottom figure in Fig. 4). In both AFM states, Weyl points do not contribute to the anomalous Hall conductivity because of the twofold rotational symmetry C_2 with the rotation axes lying in the ab plane [21]. Thus, we conclude that there probably exists a different Weyl state in $T_A < T < T_C$ no matter which type of 120° AFM order coexists with the FM order.

In summary, we report the anisotropic magnetic excitations, unusual exchange couplings, and correlations between various magnetic orders and the electronic band topology in the Weyl semimetal $\text{Co}_3\text{Sn}_2\text{S}_2$. In an intermediate temperature region $T_A < T < T_C$, a new Weyl state supported by the 120° AFM order is predicted. ARPES would be very useful to detect the Weyl points in this temperature region and to distinguish two possible 120° AFM orders. Below T_A , the simple FM order is dominated by FM third-neighbor “across-hexagon” coupling with a weak frustrated NNN bond. We further demonstrate the rigid spin approximation based calculations have shortcomings for extracting reliable magnetic exchange couplings in $\text{Co}_3\text{Sn}_2\text{S}_2$ and it requires advances in the theory of spin-spin interactions that do not rely on the existence of rigid local moments, for instance direct calculation of dynamic magnetic susceptibility from weak-coupling approaches [43,45,46].

We would like to thank Dr. S. Mankovsky for fruitful discussions. The research by S. O., J. Y., M. A. M., D. A. T. was sponsored by the Laboratory Directed Research and Development Program (LDRD) of Oak Ridge National Laboratory, managed by UT-Battelle, LLC, for the U.S. Department of Energy (Project No. 9533), with later stage supported by the U.S. DOE, Office of Science, Basic Energy Sciences, Materials Sciences and Engineering Division (J. Y.), and U.S. Department of Energy, Office

of Science, National Quantum Information Science Research Centers, Quantum Science Center (S. O., M. A. M., D. A. T.). This research used resources at Spallation Neutron Source, a DOE Office of Science User Facility operated by the Oak Ridge National Laboratory. G. D. S. was sponsored by the Laboratory Directed Research and Development Program of Oak Ridge National Laboratory, managed by UT-Battelle, LLC, for the U.S. Department of Energy. This research used resources of the Compute and Data Environment for Science (CADES) at the Oak Ridge National Laboratory, which is supported by the Office of Science of the U.S. Department of Energy under Contract No. DE-AC05-00OR22725. D. M. and R. X. acknowledge support from the Gordon and Betty Moore Foundation’s EPiQS Initiative, Grant No. GBMF9069.

*zhangq6@ornl.gov

†okapon@ornl.gov

- [1] L. Savary and L. Balents, *Rep. Prog. Phys.* **80**, 016502 (2017).
- [2] L. Balents, *Nature (London)* **464**, 199 (2010).
- [3] L. Ye *et al.*, *Nature (London)* **555**, 638 (2018).
- [4] E. Liu *et al.*, *Nat. Phys.* **14**, 1125 (2018).
- [5] M. B. Hastings, *Phys. Rev. B* **63**, 014413 (2000).
- [6] S. Yan, D. A. Huse, and S. R. White, *Science* **332**, 1173 (2011).
- [7] Y. C. He and Y. Chen, *Phys. Rev. Lett.* **114**, 037201 (2015).
- [8] O. Janson, J. Richter, and H. Rosner, *Phys. Rev. Lett.* **101**, 106403 (2008).
- [9] L. Messio, C. Lhuillier, and G. Misguich, *Phys. Rev. B* **83**, 184401 (2011).
- [10] D. Boldrin, B. Fåk, M. Enderle, S. Bieri, J. Ollivier, S. Rols, P. Manuel, and A. S. Wills, *Phys. Rev. B* **91**, 220408(R) (2015).
- [11] D. Boyko, A. Saxena, and J. T. Haraldsen, *Ann. Phys. (Amsterdam)* **532**, 1900350 (2020).
- [12] R. F. Bishop, P. H. Y. Li, D. J. J. Farnell, and C. E. Campbell, *Phys. Rev. B* **82**, 104406 (2010).
- [13] O. Janson, J. Richter, and H. Rosner, *J. Phys. Conf. Ser.* **145**, 012008 (2009).
- [14] J. S. Helton, K. Matan, M. P. Shores, E. A. Nytko, B. M. Bartlett, Y. Qiu, D. G. Nocera, and Y. S. Lee, *Phys. Rev. Lett.* **104**, 147201 (2010).
- [15] B. Fåk *et al.*, *Phys. Rev. Lett.* **109**, 037208 (2012).
- [16] D. Boldrin, B. Fåk, E. Canévet, J. Ollivier, H. C. Walker, P. Manuel, D. D. Khalyavin, and A. S. Wills, *Phys. Rev. Lett.* **121**, 107203(R) (2018).
- [17] N. Morali, R. Batabyal, P. Kumar Nag, E. Liu, Q. Xu, Y. Sun, B. Yan, C. Felser, N. Avraham, and H. Beidenkopf, *Science* **365**, 1286 (2019).
- [18] Q. Xu, E. Liu, W. Shi, L. Muechler, J. Gayles, C. Felser, and Y. Sun, *Phys. Rev. B* **97**, 235416 (2018).
- [19] J. X. Yin *et al.*, *Nat. Phys.* **15**, 443 (2019).
- [20] D. F. Liu *et al.*, *Science* **365**, 1282 (2019).
- [21] Z. Guguchia *et al.*, *Nat. Commun.* **11**, 559 (2020).
- [22] J. Legendre and K. L. Hur, *Phys. Rev. Research* **2**, 022043(R) (2020).

- [23] C. Liu *et al.*, *Sci. China Phys. Mech. Astron.* **64**, 217062 (2021). The magnetic exchange couplings S^2J were reported with the default $S = 1$. We converted them to SJ using experimental S of 0.17 as summarized in Table I.
- [24] M. A. Kassem, Y. Tabata, T. Waki, and H. Nakamura, *Phys. Rev. B* **96**, 014429 (2017).
- [25] Q. Wang, Y. Xu, R. Lou, Z. Liu, M. Li, Y. Huang, D. Shen, H. Weng, S. Wang, and H. Lei, *Nat. Commun.* **9**, 3681 (2018).
- [26] W. Schnelle, A. Leithe-Jasper, H. Rosner, F. M. Schapacher, R. Pöttgen, F. Pielhofer, and R. Weirich, *Phys. Rev. B* **88**, 144404 (2013).
- [27] See Supplemental Material at <http://link.aps.org/supplemental/10.1103/PhysRevLett.127.117201> the details of sample preparation and characterization, neutron scattering experiments, spin-wave analysis using the SpinW package, and DFT calculations, which includes Refs. [28–38].
- [28] S. Toth and B. Lake, *J. Phys. Condens. Matter* **27**, 166002 (2015).
- [29] A. F. May, J. Yan, and M. A. McGuire, *J. Appl. Phys.* **128**, 051101 (2020).
- [30] Q. Zhang *et al.*, *Phys. Rev. B* **99**, 094416 (2019).
- [31] G. Kresse and D. Joubert, *Phys. Rev. B* **59**, 1758 (1999).
- [32] J. P. Perdew, K. Burke, and M. Ernzerhof, *Phys. Rev. Lett.* **77**, 3865 (1996).
- [33] G. Kresse and J. Furthmüller, *Phys. Rev. B* **54**, 11169 (1996).
- [34] H. Ebert, D. Ködderitzsch, and J. Minár, *Rep. Prog. Phys.* **74**, 096501 (2011).
- [35] H. Ebert *et al.*, Munich SPR-KKR package, version 7.7, <http://olymp.cup.uni-muenchen.de/ak/ebert/SPRKKR>, 2017.
- [36] A. I. Liechtenstein, V. I. Anisimov, and J. Zaanen, *Phys. Rev. B* **52**, R5467 (1995).
- [37] Q. S. Wu, S. N. Zhang, H.-F. Song, M. Troyer, and A. A. Soluyanov, *Comput. Phys. Commun.* **224**, 405 (2018).
- [38] G. Pizzi *et al.*, *J. Phys. Condens. Matter* **32**, 165902 (2020).
- [39] P. Vaquero and G. G. Sobany, *Solid State Sci.* **11**, 513 (2009).
- [40] A. I. Liechtenstein, M. I. Katsnelson, V. P. Antropov, and V. A. Gubanov, *J. Magn. Magn. Mater.* **67**, 65 (1987).
- [41] H. Ebert and S. Mankovsky, *Phys. Rev. B* **79**, 045209 (2009).
- [42] D. M. Korotin, V. V. Mazurenko, V. I. Anisimov, and S. V. Streltsov, *Phys. Rev. B* **91**, 224405 (2015).
- [43] P. Buczek, A. Ernst, and L. M. Sandratskii, *Phys. Rev. B* **84**, 174418 (2011).
- [44] M. van Schilfgaarde and V. P. Antropov, *J. Appl. Phys.* **85**, 4827 (1999).
- [45] T. Izuyama, D. Kim, and R. Kubo, *J. Phys. Soc. Jpn.* **18**, 1025 (1963).
- [46] S. Y. Savrasov, *Phys. Rev. Lett.* **81**, 2570 (1998).